Journal of Alloys and Compounds 509 (2011) 7553–7558

Contents lists available at ScienceDirect

Journal of Alloys and Compounds

journal homepage: www.elsevier.com/locate/jallcom

Crystal structure change in the dehydrogenation process of the Li–Mg–N–H system

T. Noritake[a,*], M. Aoki[a], M. Matsumoto[a], K. Miwa[a], S. Towata[a], H.-W. Li[b], S. Orimo[b]

[a] Toyota Central R&D Labs., Inc., Nagakute, Aichi 480-1192, Japan
[b] Institute for Materials Research, Tohoku University, Sendai 980-8577, Japan

ARTICLE INFO

Article history:
Received 9 December 2009
Received in revised form 13 April 2011
Accepted 15 April 2011
Available online 23 April 2011

Keywords:
Hydrogen storage materials
Complex hydride
X-ray diffraction
Synchrotron radiation

ABSTRACT

The Li–Mg–N–H system has the property of reversible reaction with hydrogen between hydrogenation and dehydrogenation ($Mg_3N_2 + 4Li_3N + 12H_2 \leftrightarrow 3Mg(NH_2)_2 + 12LiH$). At the several dehydrogenation stages of p–c isotherm measurement at 523 K, the structural change was investigated using the synchrotron X-ray diffraction. There are two regions in p–c isotherm of the Li–Mg–N–H system, i.e. plateau and sloping region. In the plateau region, $Mg(NH_2)_2$ and $Li_3Mg_3(NH_2)(NH)_4$ coexist. In the sloping region, the intermediate phase $Li_{3+3y}Mg_3(NH_2)_{1-y}(NH)_{4+2y}$ changes continuously from $Li_3Mg_3(NH_2)(NH)_4$ to $Li_2Mg(NH)_2$. The chemical composition of the intermediate phase was estimated from the amount of desorbed hydrogen by p–c isotherm and the atomic ratio of Mg and N by Rietveld analysis. The crystal structure of the intermediate phase, $Li_{3+3y}Mg_3(NH_2)_{1-y}(NH)_{4+2y}$ (space group: *I*222), was determined. Because all these intermediate structures are similar to anti-CaF_2-type, it is deduced that the dehydrogenation process are caused by the diffusion of Li^+ to cation sites of $Mg(NH_2)_2$. The analysis of structural change clarified the dehydrogenation process that is accomplished by the diffusion of Li^+ and Mg^{2+} without N atom diffusion.

© 2011 Elsevier B.V. All rights reserved.

1. Introduction

Hydrogen storage technology is one of the most important subjects for the widespread practical use of fuel cell vehicles. Light element complex hydrides, such as alanates, amides and borohydrides, are attracted a great deal of attention as new materials for safe and efficient hydrogen storage [1]. Especially, in Li–N–H system, reversible hydrogen storage is possible among lithium nitride, lithium imide and lithium amide [2,3].

$$LiNH_2 + 2LiH \leftrightarrow Li_2NH + LiH + H_2 \leftrightarrow Li_3N + 2H_2 \quad (1)$$

It is necessary to lower the temperature of this reaction for the practical use. As the effective method of lowering the reaction temperature, the destabilization of $LiNH_2$ to substitute Li partially by elements with larger electronegativity, such as Mg, was proposed [4–6]. For further development of the study, it was found that the mixture of $Mg_3N_2 + 4Li_3N$ possesses reversible hydrogen storage functions in which 9.1 mass% of hydrogen can be stored [7,8].

$$3Mg(NH_2)_2 + 12LiH \leftrightarrow Mg_3N_2 + 4Li_3N + 12H_2 \quad (2)$$

In this Li–Mg–N–H system, the intermediate phase $Li_2Mg(NH)_2$ is formed in the reaction process by the following reaction formula.

$$3Mg(NH_2)_2 + 12LiH \leftrightarrow 3Li_2Mg(NH)_2 + 6LiH + 6H_2 \quad (3)$$

The researches with different compositions or different starting materials were reported as to the Li–Mg–N–H system [9–11]. Because of the high hydrogen density and the reversibility of reaction, it is currently considered that the Li–Mg–N–H system is one of the most promising candidates for new hydrogen storage materials. The numerous researches have been reported as to the reversible reaction mechanism of the Li–Mg–N–H system [12–16]. Especially, as for the intermediate phases during the reaction process, in situ measurement of structural change [17–21], theoretical calculation [22,23] and thermal stability [24] have been advanced. However, the reversible reaction mechanism under hydrogen pressure has not been sufficiently clarified, yet. There are unknown structures in intermediate phases creating under hydrogen pressure. Therefore, the crystal structure analyses in the dehydrogenation process of the Li–Mg–N–H system have been performed for understanding of the reaction mechanism.

2. Experimental

The experimental details regarding the sample preparation and pressure–composition (p–c) isotherm measurement were described in the previous paper [25]. Starting materials of Mg_3N_2 and Li_3N were synthesized using a Mo crucible by gas phase nitrogenation of Mg metal and Li metal (Sigma–Aldrich),

* Corresponding author. Tel.: +81 561 71 7804; fax: +81 561 63 6136.
E-mail address: e0553@mosk.tytlabs.co.jp (T. Noritake).

0925-8388/$ – see front matter © 2011 Elsevier B.V. All rights reserved.
doi:10.1016/j.jallcom.2011.04.079

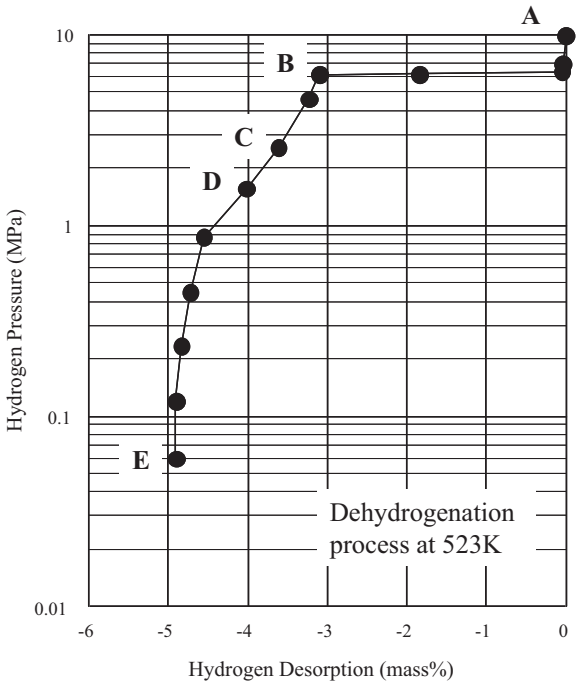

Fig. 1. The p–c isotherm during dehydrogenation process at 523 K for the mixture of $Mg_3N_2 + 4Li_3N$ after hydrogenation. The hydrogen desorption is represented by mass fraction for $Mg_3N_2 + 4Li_3N$.

respectively. The mixture of $Mg_3N_2 + 4Li_3N$ was mechanically milled for 1 h under argon atmosphere using a planetary ball mill (Fritsch P-7). The mixture sample was hydrogenated at hydrogen pressure 9.5 MPa and then p–c isotherm measurement during the dehydrogenation process was performed at 523 K using the conventional Sieverts apparatus (Suzuki Shokan Co., Ltd.). At the several dehydrogenation stages of p–c isotherm measurement, the sample was taken out from the apparatus and then was preserved in a glove-box filled with purified argon (dew point below 180 K). As the taking-out procedure from the apparatus, firstly cooling down to room temperature was executed and secondly hydrogen pressure was lowered to 0.1 MPa. It is expected that there is almost no change of hydrogen composition in the sample during this procedure.

The diffraction intensities from hydrogen and lithium atoms are very weak, and so the highly brilliant X-ray source of synchrotron radiation (SPring-8) was used for the diffraction measurement. The powder sample was inserted into a glass capillary (diameter: 0.3 mm) and then was sealed by an epoxy adhesive. The synchrotron X-ray diffraction measurement was carried out by use of a large Debye–Scherrer camera with an imaging plate as detectors at the beam-line BL19B2 of SPring-8 [26]. The measurement data were collected at room temperature using the incident X-ray wavelength with 0.80 Å (for samples A, B and E) and 1.0 Å (for samples C and D). The crystal structure analysis was accomplished by the Rietveld method using the computer program RIETAN [27].

3. Results and discussion

3.1. Chemical composition of the intermediate phases

The result of p–c isotherm measurement at 523 K and the sampling points are shown in Fig. 1. At each sampling point of A, B, C, D and E, the measured value of the desorbed hydrogen are 0.0, 3.1, 3.5, 4.0 and 4.9 mass% (0.0, 3.7, 4.2, 4.8, 5.8 mol%) for $Mg_3N_2 + 4Li_3N$, respectively. The level of impurities in the sample is unconfirmed, but samples are surely containing small amount of impurities, such as MgO. By taking account of the existence of impurities, it is estimated that the amounts of the desorbed hydrogen is approximately 4.0, 4.4, 5.0 and 6.0 mol% at B, C, D and E, respectively. In the previous study [25,28], the chemical formula of intermediate phase in sample B was estimated to $Li_4Mg_3(NH_2)_2(NH)_4$ according to the amount of the desorbed hydrogen during p–c isotherm measurement. In this chemical composition, the atomic ratio of Mg and N is 3:6. The result of Rietveld analysis using this composition was

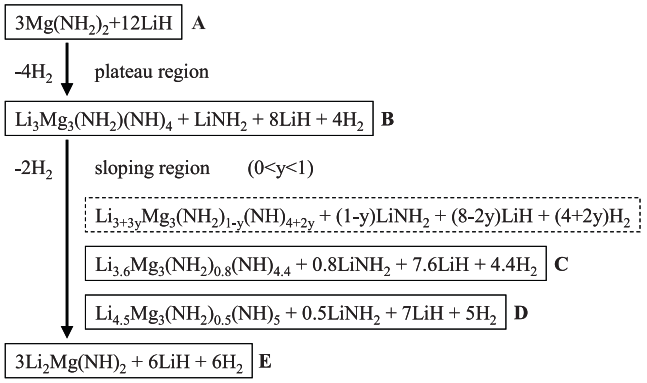

Fig. 2. The dehydrogenation process for the mixture of $Mg_3N_2 + 4Li_3N$ after hydrogenation (namely, $3Mg(NH_2)_2 + 12LiH$) based on the results of the p–c isotherm measurement and Rietveld analysis. Points A, B, C, D, and E correspond to those shown in Fig. 1, respectively.

less agreement between observed and calculated diffraction intensities. To improve the agreement, occupancy parameters of Mg in Rietveld analysis were refined. The better analysis result was obtained in 3:5 for the atomic ratio of Mg and N. In addition, $LiNH_2$ phase was contained in the sample B. Therefore, it is conceivable that $Li_4Mg_3(NH_2)_2(NH)_4$ was divided into $Li_3Mg_3(NH_2)(NH)_4$ and $LiNH_2$. The chemical formula of intermediate phase in sample B is revalued to $Li_3Mg_3(NH_2)(NH)_4$. The reaction in the plateau region is represented as the following formula.

$$3Mg(NH_2)_2 + 12LiH \leftrightarrow Li_3Mg_3(NH_2)(NH)_4 + LiNH_2 + 8LiH + 4H_2 \quad (4)$$

The four phases, $Mg(NH_2)_2$, $Li_3Mg_3(NH_2)(NH)_4$, $LiNH_2$, and LiH, coexist in plateau region and the phase ratio changes according to the amount of the desorbed hydrogen. In the same way, the atomic ratio of Mg and N in the Li–Mg–N–H intermediate phase for samples C and D was estimated by the Rietveld analysis. As the result, the reaction in the sloping region is represented as follows:

$$\begin{gathered} Li_3Mg_3(NH_2)(NH)_4 + LiNH_2 + 8LiH + 4H_2 \quad (y = 0) \\ \updownarrow \\ Li_{3+3y}Mg_3(NH_2)_{1-y}(NH)_{4+2y} + (1-y)LiNH_2 + (8-2y)LiH \\ +(4+2y)H_2 \quad (0 < y < 1) \\ \updownarrow \\ 3Li_2Mg(NH)_2 + 6LiH + 6H_2 \quad (y = 1) \end{gathered} \quad (5)$$

The value of y in this formula changes from 0 to 1. Namely, the composition of the intermediate phase $Li_{3+3y}Mg_3(NH_2)_{1-y}(NH)_{4+2y}$ changes continuously in sloping region. This continuous composition change causes the sloping shape in p–c isotherm curve. The reaction formulas that estimated by the amounts of the desorbed hydrogen and Rietveld analysis are summarized in Fig. 2.

3.2. Crystal structure of $Li_{3+3y}Mg_3(NH_2)_{1-y}(NH)_{4+2y}$

The Rietveld analysis patterns for the samples B, C and E are shown in Figs. 3–5. The diffraction pattern for sample D was similar to that for sample C and so its figure was omitted. Unfortunately, Li_2O, LiOH and MgO are included in large quantities in these samples. As this cause, it is presumed that the seal of capillary or the sample reservation was insufficient. In addition, there is a trace of Fe and Mo for impurities mixed during the sample preparation. The results of Rietveld analysis could obtain high reliability and determine the intermediate crystal structures. The reliability factors of Rietveld analysis and the content ratio of crystal phase are inserted in Figs. 3–5. At the early stage of analysis, the crystal structures are analyzed without hydrogen atoms. On the assumption

Table 1
$Li_3Mg_3(NH_2)(NH)_4$ crystallographic data.

Chemical composition:		$Li_{4.8}Mg_{4.8}N_8H_{9.6}$			
Space group:		$I\bar{4}2m$ (No. 121)			
Lattice constant (Å):		a = 5.1461(4)		c = 9.5817(7)	
Atom	g	x	y	z	B_{iso} (Å^2)
Mg1	0.867(3)	0.0	0.0	0.0	0.87(4)
Li1	0.133	0.0	0.0	0.0	0.87
Mg2	0.767	0.0	0.5	0.25	1.09(3)
Li2	0.233	0.0	0.5	0.25	1.09(8)
Li3	0.141	0.0	0.5	0.0	0.64
Li4	0.759(6)	0.0	0.0	0.2662(5)	0.64(8)
N	1.0	0.2301(3)	0.2301	0.1396(2)	1.70(4)
H1	0.55	0.325(5)	0.325	0.066(4)	1.70
H2	0.32	0.340	0.120	0.090	1.70

R_{wp} = 2.37%, R_R = 8.10%, R_I = 2.97%, S = 2.778.

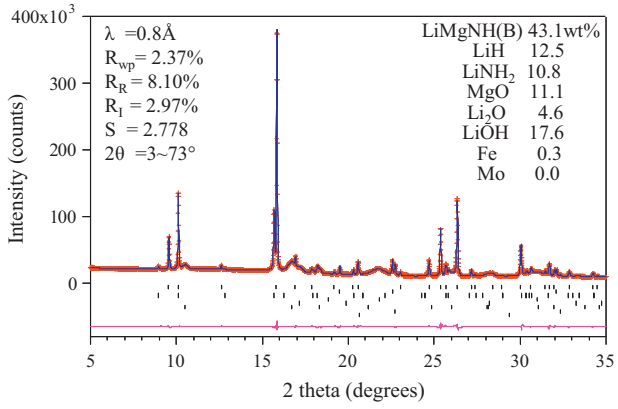

Fig. 3. The Rietveld analysis pattern of sample B. X-ray wave length is 0.8 Å.

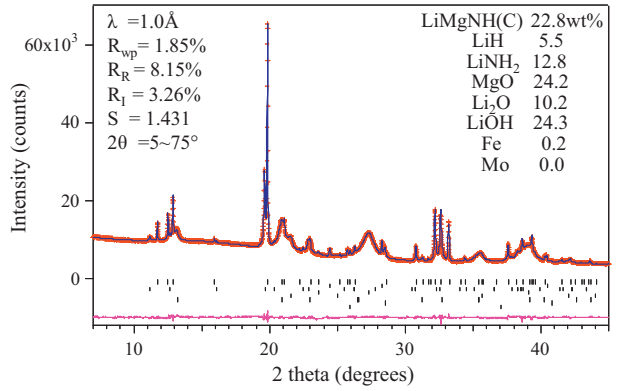

Fig. 4. The Rietveld analysis pattern of sample C. X-ray wave length is 1.0 Å.

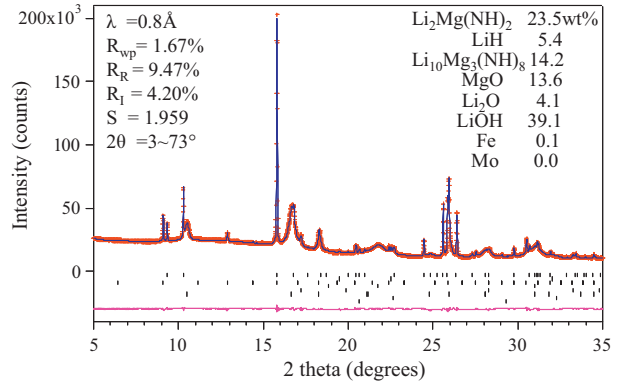

Fig. 5. The Rietveld analysis pattern of sample E. X-ray wave length is 0.8 Å.

that there is no vacancy in N atom sites, the occupancies of cation site are analyzed. The occupancy parameters of Mg, Li and H are refined under the constrained condition to agree with the chemical composition determined by the amount of the desorbed hydrogen (Fig. 2). At the beginning of analysis, the atomic coordinates of hydrogen in NH_2 and NH were fixed at the distance 1.0 Å from N atom in the direction to the vacant cation site, and finally were refined. The isotropic atomic displacement parameters of N and H, B_{iso}, are constrained to the same value. The parameters that dose not converged in the final refinement were partially constrained or fixed.

The obtained crystallographic data of $Li_3Mg_3(NH_2)(NH)_4$, $Li_{3.6}Mg_3(NH_2)_{0.8}(NH)_{4.4}$, $Li_{4.5}Mg_3(NH_2)_{0.5}(NH)_5$ and $Li_2Mg(NH)_2$ are listed in Tables 1–4, respectively. The space groups of $Li_3Mg_3(NH_2)(NH)_4$, $Li_{3+3y}Mg_3(NH_2)_{1-y}(NH)_{4+2y}$ and $Li_2Mg(NH)_2$ are different each other ($I\bar{4}2m$, $I222$ and $Ibam$) but representing these three crystal structures by space group $I222$ is possible. Namely, $Li_{3+3y}Mg_3(NH_2)_{1-y}(NH)_{4+2y}$ can change continuously from $Li_3Mg_3(NH_2)(NH)_4$ to $Li_2Mg(NH)_2$. The crystal structures of the phase containing Mg in each sample are shown in Fig. 6.

These crystal structures are similar to anti-CaF_2 type. The anions, NH_2^- or NH^{2-}, compose FCC-type arrangement and the cations, Mg^{2+} or Li^+, are located in the interstitial sites. Nitrogen atoms coordinate in tetrahedral sites around the cations. The crystal structure of $Mg(NH_2)_2$ in sample A, which structure is already known [29,30], also resembles anti-CaF_2 type. There are eight cation sites in anti-CaF_2 type structure. In $Mg(NH_2)_2$, Mg^{2+} ions are located in the two cation sites and the other six cation sites are vacant. In the intermediate phase $Li_{3+3y}Mg_3(NH_2)_{1-y}(NH)_{4+2y}$ formed during the dehydrogenation process, Mg^{2+} and Li^+ ions are randomly distributed in the cation sites. These cation sites consist of Mg-rich, Li-rich and vacant sites according to the chemical composition. Fig. 7 shows the crystal structure of $Li_{3+3y}Mg_3(NH_2)_{1-y}(NH)_{4+2y}$ and the cation site name. The occupancy rates of Mg^{2+} and Li^+ in eight cation sites estimated by the Rietveld analysis are listed in Table 5. In $Li_3Mg_3(NH_2)(NH)_4$, Li3 site and Va1 site are equivalent and lattice constants b and c are the same length. The occupancy rates of Li^+ in the intermediate phase increase with decreasing hydrogen concentration by dehydrogenation. Because the occupancy rates of Li3 site and Li4 site increases especially, the lattice constant c increases in length. In $Li_2Mg(NH)_2$, Mg^{2+} and Li^+ ions distribute in Li3 and Li4 sites. Consequently, Mg1 site and Li3 site, together with Mg2 site and Li4 site, become equivalent. Thus the intermediate phase $Li_{3+3y}Mg_3(NH_2)_{1-y}(NH)_{4+2y}$ changes continuously from $Li_3Mg_3(NH_2)(NH)_4$ to $Li_2Mg(NH)_2$ by the different distributions of Mg^{2+} and Li^+. In sample E, the $LiNH_2$ phase disappears, but cubic phase which crystal structure is similar to β-$Li_2Mg(NH)_2$ [19] appears. The chemical composition of this cubic phase was estimated by Rietveld analysis and so was represented

Table 2
$Li_{3.6}Mg_3(NH_2)_{0.8}(NH)_{4.4}$ crystallographic data.

Chemical composition		$Li_{5.54}Mg_{4.62}N_8H_{9.23}$			
Space group:		*I*222 (No. 23)			
Lattice constant (Å):		$a = 9.7492(11)$	$b = 4.9930(6)$	$c = 5.1788(6)$	
Atom	*g*	*x*	*y*	*z*	B_{iso} (Å^2)
Mg1	0.896(8)	0.0	0.0	0.0	1.34(10)
Li1	0.104	0.0	0.0	0.0	1.34
Mg2	0.706	0.2572(3)	0.0	0.5	1.27(8)
Li2	0.294	0.2572	0.0	0.5	1.27
Li3	0.75(2)	0.0	0.0	0.5	1.06(14)
Li4	0.66	0.2681(12)	0.0	0.0	1.06
N	1.0	0.1350(4)	0.2216(6)	0.2389(15)	1.70(8)
H1	0.87(7)	0.073(6)	0.340(9)	0.351(8)	1.70
H2	0.28	0.136(13)	0.325(21)	0.053(40)	1.70

$R_{wp} = 1.85\%$, $R_R = 8.15\%$, $R_I = 3.26\%$, $S = 1.431$.

Table 3
$Li_{4.5}Mg_3(NH_2)_{0.5}(NH)_5$ crystallographic data.

Chemical composition:		$Li_{6.55}Mg_{4.36}N_8H_{8.73}$			
Space group:		*I*222 (No. 23)			
Lattice constant (Å):		$a = 9.7834(16)$	$b = 4.9748(8)$	$c = 5.1881(8)$	
Atom	*g*	*x*	*y*	*z*	B_{iso} (Å^2)
Mg1	0.862(10)	0.0	0.0	0.0	1.22(15)
Li1	0.138	0.0	0.0	0.0	1.22
Mg2	0.660	0.2573(4)	0.0	0.5	0.96(10)
Li2	0.340	0.2573	0.0	0.5	0.96
Li3	1.0	0.0	0.0	0.5	1.50
Li4	0.727	0.2689(17)	0.0	0.0	1.50
N	1.0	0.1318(7)	0.2150(8)	0.2397(15)	1.41(11)
H1	0.83(6)	0.126(6)	0.336(11)	0.379(12)	1.41
H2	0.26	0.081	0.335	0.120	1.41

$R_{wp} = 1.70\%$, $R_R = 7.17\%$, $R_I = 2.65\%$, $S = 1.322$.

Table 4
$Li_2Mg(NH)_2$ crystal data.

Chemical composition:		$Li_8Mg_4N_8H_8$			
Space group:		*Iba*2 (No. 45)			
Lattice constant (Å):		$a = 9.8044(8)$	$b = 5.0006(4)$	$c = 5.2091(4)$	
Atom	*g*	*x*	*y*	*z*	B_{iso} (Å^2)
Mg1	0.442(4)	0.0	0.0	0.0	1.86(9)
Li1	0.558	0.0	0.0	0.0	1.86
Mg2	0.289	0.2394(2)	0.5005(28)	0.4985(56)	1.06(7)
Li2	0.721	0.2394	0.5005	0.4985	1.06
N	1.0	0.1350(4)	0.2216(6)	0.2389(15)	0.64(5)
H1	1.0	0.136(13)	0.325(21)	0.053(40)	4.4(20)

$R_{wp} = 1.67\%$, $R_R = 9.47\%$, $R_I = 4.20\%$, $S = 1.959$.

as $Li_{10}Mg_3(NH)_8$. This chemical composition is relatively close to $Li_{2.6}MgN_2D_{1.4}$ that was analyzed by in situ neutron diffraction [20]. The cubic structure $Li_{10}Mg_3(NH)_8$ is found in the case with inadequate reaction. If reacting adequately, it is expected that only $Li_2Mg(NH)_2$ is created at dehydrogenation state (sampling point E). Therefore, the dehydrogenation mechanism (next section) is discussed in absence of $Li_{10}Mg_3(NH)_8$ phase. The crystal structures of $Li_2Mg(NH)_2$ and $Li_3Mg_3(NH_2)(NH)_4$ are almost the same with those of α-$Li_2Mg(NH)_2$ [19] and $Li_2Mg_2(NH)_3$ [21], which have been already reported. In the present study, the crystal structure of $Li_{3+3y}Mg_3(NH_2)_{1-y}(NH)_{4+2y}$ was determined for the first time.

Table 5
Occupancy rate of eight cation sites in the intermediate phases.

	Site name	Mg1	Li3	Va1	Va2	Mg2	Mg2	Li4	Li4
Sample B	g:Mg	0.87	0.00	0.00	0.00	0.77	0.77	0.00	0.00
$Li_{4.8}Mg_{4.8}N_8H_{9.6}$	g:Li	0.13	0.14	0.14	0.00	0.23	0.23	0.76	0.76
Sample C	g:Mg	0.90	0.00	0.00	0.00	0.71	0.71	0.00	0.00
$Li_{5.54}Mg_{4.62}N_8H_{9.23}$	g:Li	0.10	0.75	0.00	0.00	0.29	0.29	0.66	0.66
Sample D	g:Mg	0.86	0.00	0.00	0.00	0.66	0.66	0.00	0.00
$Li_{6.55}Mg_{4.36}N_8H_{8.73}$	g:Li	0.14	1.00	0.00	0.00	0.34	0.34	0.73	0.73
Sample E	g:Mg	0.44	0.44	0.00	0.00	0.28	0.28	0.28	0.28
$Li_8Mg_4N_8H_8$	g:Li	0.56	0.56	0.00	0.00	0.72	0.72	0.72	0.72

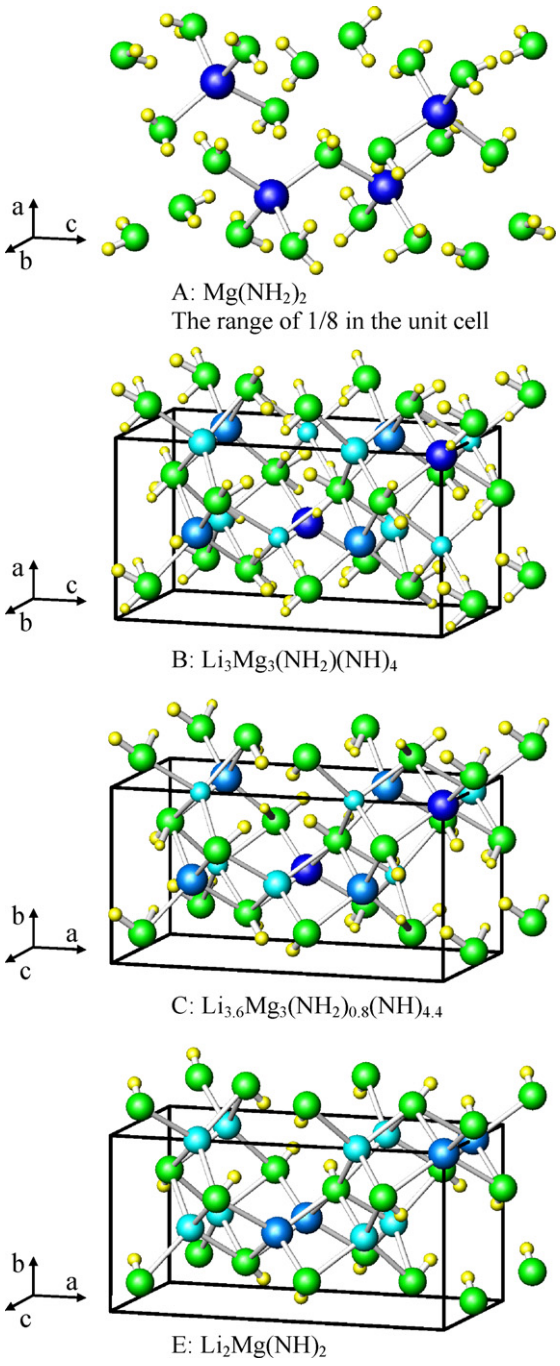

Fig. 6. Crystal structures of the phase containing Mg in each sample. $Li_{4.5}Mg_3(NH_2)_{0.5}(NH)_5$ in sample D is omitted because of almost the same with sample C. Mg-rich: dark blue, Li-rich: blue, Li: light blue, N: light green, H: yellow, small sphere of Li and H: small occupancy. (For interpretation of the references to color in this figure legend, the reader is referred to the web version of this article.)

3.3. Dehydrogenation mechanism in the Li–Mg–N–H system

As the result of the crystal structure analysis during the dehydrogenation process (Fig. 6), it is considered that the dehydrogenation reaction is caused by the diffusion of Li^+ in cation sites of $Mg(NH_2)_2$. LiH is a very stable compound but has a reactive property with other hydrides, for example, LiH + $LiNH_2$ [2,3]. The expected reaction process in the Li–Mg–N–H system is illustrated schematically in Fig. 8. Namely, Li^+ ion diffuses from LiH to $Mg(NH_2)_2$ crystal and then decomposes NH_2^- into NH^{2-} and H^+. The created H^+ combines with H^- on the side of LiH and H_2 gas is released. It has been confirmed that the isotherm during re-hydrogenation is similar to that during dehydrogenation and the observed hysteresis is small in the Li–Mg–N–H system [31]. Therefore, the hydrogenation reacts probably with the reverse process, which begins with the dissociation of hydrogen molecule.

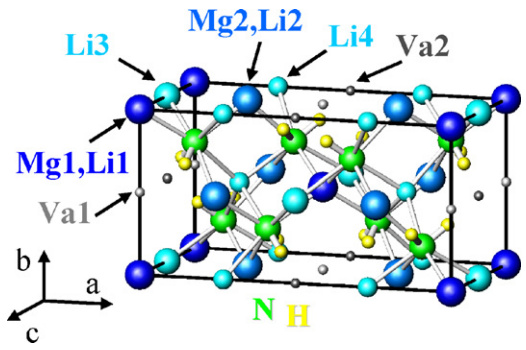

Fig. 7. The arrangement of atom and vacancy sites in $Li_{3.6}Mg_3(NH_2)_{0.8}(NH)_{4.4}$.

$Li_2Mg_2(NH)_3$ [17,21,24] is already known as the intermediate phase created during the reaction process from $Mg(NH_2)_2$ to $Li_2Mg(NH)_2$. Assuming that $Li_2Mg_2(NH)_3$ forms in the present case of $3Mg(NH_2)_2 + 12LiH$, the reaction in plateau and sloping region is represented by formula (6) and (7), respectively.

$$3Mg(NH_2)_2 + 12LiH \leftrightarrow 1.5Li_2Mg_2(NH)_3 + 1.5LiNH_2 + 7.5LiH + 4.5H_2 \quad (6)$$

$$1.5Li_2Mg_2(NH)_3 + 1.5LiNH_2 + 7.5LiH + 4.5H_2 \leftrightarrow 3Li_2Mg(NH)_2 + 6LiH + 6H_2 \quad (7)$$

The amount of desorbed hydrogen at the point B, $4.0H_2$, disagrees with the value of formula (6), $4.5H_2$. It is conceivable that $Li_3Mg_3(NH_2)(NH)_4$ consisting of amide and imide is more unstable than $Li_2Mg_2(NH)_3$ consisting of only imide but is able to exist as a stable phase at high pressure in hydrogen atmosphere. In the present case, $Li_3Mg_3(NH_2)(NH)_4$ is formed according to the reaction formula showing in Fig. 2. Therefore, the following reaction process is expected.

1. By the dehydrogenation, Li^+ ion diffuses in $Mg(NH_2)_2$ phase from LiH phase and NH_2^- changes into NH^{2-} (Fig. 8).
2. In the high-pressure hydrogen atmosphere, NH_2^- dose not fully changes into NH^{2-} and remains partially. At the same time, the Li rich area and Mg rich area in $Mg(NH_2)_2$ phase are generated by the diffusion of Li^+ and Mg^{2+}.
3. Because the crystal structure of $LiNH_2$ also resemble anti-CaF_2 type [30] in common with $Mg(NH_2)_2$, $LiNH_2$ and $Li_3Mg_3(NH_2)(NH)_4$ are generated from the Li rich and Mg rich area, respectively. Namely, $Mg(NH_2)_2$ phase separates into these two phases by the diffusion of Li^+ and Mg^{2+} without N atom diffusion.

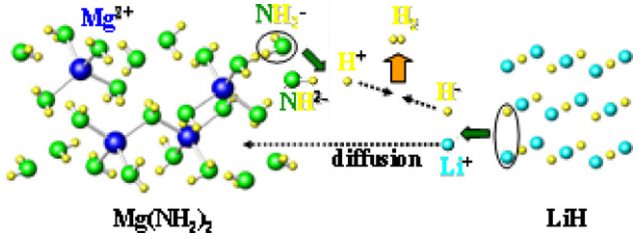

Fig. 8. Schematic illustration of dehydrogenation process in the Li–Mg–N–H system.

4. Because the remained NH_2^- changes into NH^{2-} continuously along with dehydrogenation, $LiNH_2$ decreases gradually and $Li_3Mg_3(NH_2)(NH)_4$ is transformed continuously to $Li_2Mg(NH)_2$ in the sloping region. The transformation from $LiNH_2$ and $Li_3Mg_3(NH_2)(NH)_4$ to $Li_2Mg(NH)_2$ are also accomplished by the diffusion of Li^+ and Mg^{2+} without N atom diffusion because of these structure similarity. The reaction formulas of plateau and sloping region in p–c isotherm are represented as (4) and (5), not (6) and (7).

4. Conclusion

The crystal structure changes during dehydrogenation process in the Li–Mg–N–H system are analyzed by ex situ X-ray diffraction measurement. As the result, all crystal structures formed in this process are similar to anti-CaF_2 type and the occupancy rate of Li and Mg in cation sites changes with the dehydrogenation process. Therefore, the dehydrogenation reaction is caused by the diffusion of Li^+ into $Mg(NH_2)_2$. There are the plateau are sloping region in p–c isotherm of dehydrogenation process. In the plateau region, $Mg(NH_2)_2$ and $Li_3Mg_3(NH_2)(NH)_4$ coexist and these phase ratio changes by dehydrogenation. In the sloping region, the crystal structure of $Li_{3+3y}Mg_3(NH_2)_{1-y}(NH)_{4+2y}$ changes continuously. Furthermore, the structural similarity of imide and amide compounds in the Li–Mg–N–H system is one of the factors for reversible reaction.

Acknowledgements

The synchrotron radiation experiments were carried out on BL19B2 of the SPring-8 with the approval of the Japan Synchrotron Radiation Research Institute (JASRI) (Proposal Nos. 2005A0152-NI-np, 2005B0897-NI-np). This work was partially supported by the New Energy and Industrial Technology Development Organization (NEDO). The authors express their heartfelt thanks to Mr. G. Kitahara, Ms. N. Ohba and Dr. Y. Nakamori for their valuable support and discussion.

References

[1] S. Orimo, Y. Nakamori, J.R. Eliseo, A. Züttel, C.M. Jensen, Chem. Rev. 107 (2007) 4111.
[2] P. Chen, Z.T. Xiong, J.Z. Luo, J.Y. Lin, K.L. Tan, Nature 420 (2002) 302.
[3] P. Chen, Z. Xiong, J. Luo, J. Lin, K.L. Tan, J. Phys. Chem. B 107 (2003) 10967.
[4] Y. Nakamori, S. Orimo, J. Alloys Compd. 370 (2004) 271.
[5] Y. Nakamori, S. Orimo, Mater. Sci. Eng. B 108 (2004) 48.
[6] S. Orimo, K. Nakamori, G. Kitahara, K. Miwa, N. Ohba, Y. Noritake, S. Towata, Appl. Phys. A 79 (2004) 1765.
[7] Y. Nakamori, G. Kitahara, S. Orimo, J. Power Sources 138 (2004) 309.
[8] Y. Nakamori, G. Kitahara, K. Miwa, S. Towata, S. Orimo, Appl. Phys. A 80 (2005) 1.
[9] Z.T. Xiong, G.T. Wu, J.J. Hu, P. Chen, Adv. Mater. 16 (2004) 1522.
[10] W. Luo, J. Alloys Compd. 381 (2004) 284.
[11] H. Leng, T. Ichikawa, S. Hino, N. Hanada, S. Isobe, H. Fujii, J. Phys. Chem. B 108 (2004) 8763.
[12] H. Leng, T. Ichikawa, S. Hino, T. Nakagawa, H. Fujii, J. Phys. Chem. B 109 (2005) 10744.
[13] P. Chen, Z. Xiong, L. Yang, G. Wu, W. Luo, J. Phys. Chem. B 110 (2006) 14221.
[14] R. Janot, J. Eymery, J. Tarascon, J. Power Sources 164 (2007) 496.
[15] W. Lohstroh, M. Fichtner, J. Alloys Compd. 446–447 (2007) 332.
[16] J. Wang, H. Li, S. Wang, X. Liu, Y. Li, L. Jiang, Int. J. Hydrogen Energy 34 (2009) 1411.
[17] J. Hu, Y. Liu, G. Wu, Z. Xiong, P. Chen, J. Phys. Chem. C 111 (2007) 18439.
[18] T. Nakagawa, T. Ichikawa, R. Iida, H. Leng, N.o. Takeichi, T. Kiyobayashi, H. Takeshita, H. Fujii, J. Alloys Compd. 430 (2007) 217.
[19] J. Rijssenbeek, Y. Gao, J. Hanson, Q. Juang, C. Jones, B. Toby, J. Alloys Compd. 454 (2007) 233.
[20] Y. Nakamura, S. Hino, T. Ichikawa, H. Fujii, H.W. Brinks, B.C. Hauback, J. Alloys Compd. 457 (2008) 362.
[21] E. Weidner, F. Dolci, J. Hu, W. Lohstroh, T. Hansen, D. Bull, M. Fichtner, J. Phys. Chem. C 113 (2009) 15772.
[22] Y. Wang, M.Y. Chou, Phys. Rev. B 76 (2007) 014116.
[23] K. Michel, A. Akbarzadeh, V. Ozolins, J. Phys. Chem. C 113 (2009) 14551.
[24] J. Hu, M. Fichtner, Chem. Mater. 21 (2009) 3485.
[25] M. Aoki, T. Noritake, G. Kitahara, Y. Nakamori, S. Towata, S. Orimo, J. Alloys Compd. 428 (2007) 307.
[26] E. Nishibori, M. Takata, K. Kato, M. Sakata, Y. Kubota, S. Aoyagi, Y. Kuroiwa, M. Yamakata, N. Ikeda, Nucl. Instrum. Meth. A 467–468 (2001) 1045.
[27] F. Izumi, T. Ikeda, Mater. Sci. Forum 321–324 (2000) 198.
[28] T. Noritake, M. Aoki, S. Towata, Y. Nakamori, S. Orimo, MRS Proc. 971 (2006) Z05–Z07.
[29] H. Jacobs, Z. Anorg. Allg. Chem. 382 (1971) 97–109.
[30] M. Sorby, Y. Nakamura, H. Brinks, T. Ichikawa, S. Hino, H. Fujii, B.C. Hauback, J. Alloys Compd. 428 (2007) 297.
[31] M. Aoki, T. Noritake, Y. Nakamori, S. Towata, S. Orimo, J. Alloys Compd. 446–447 (2007) 328–331.